

Emergent Weyl Semi-Metal in a Paired Topological Superfluidity

Ching-Yu Huang,¹ Jiapei Zhuang,² and Daw-Wei Wang^{2,3}

¹*Department of Applied Physics, Tunghai University, Taichung 40704, Taiwan*

²*Department of Physics, National Tsing Hua University, Hsinchu 30013, Taiwan*

³*National Center for Theoretical Sciences, Hsinchu 30013, Taiwan*

(Dated: July 30, 2020)

In this paper, we systematically investigate the topological properties of a paired 2D *p*-wave superfluids, where spin polarized fermionic atoms are loaded in a bilayer optical lattice with a weak coupling to Rydberg excited states. By changing the strength of Rydberg coupling as well as the inter-layer spacing, we find that there could be a finite parameter regime, where the intra-plane *p*-wave pairing could co-exist with the inter-plane *s*-wave pairing, leading to a gapless phase of topological properties. The ground state is found to be a Weyl semi-metal with a flat band (Fermi arch) at the boundary. We show that such quantum and topological phase transition could be further understood from symmetry properties as well as the effective 1D Kitaev ladders with four legs.

I. INTRODUCTION

In this paper, we would like to study the two order parameters appears in two-dimensional(2D) bilayer fermionic system.

We can tune the Rydberg blockade radius to be smaller or larger than several inter-layer distance, giving intra-layer or longer-ranged inter-layer *p*-wave pairing and transitions between various topological states.

A Majorana fermion (MF) is known to be its own antiparticle¹, as a hypothesis in theoretical particle physics. In condensed matter systems, a MF can appear as a localized edge state, reflecting the topological order (TO) in the bulk of system. It is known that systems of topological order can be classified into intrinsic TO or symmetry-protected topological (SPT) order: the latter is robust against local perturbations for a given on-site symmetries². Ground states of nontrivial SPT phases cannot be continuously connected to trivial product states without either closing the gap or breaking the protecting symmetry³.

One of the mostly studied TO phase is proposed by Kitaev⁴ for one-dimensional (1D) *p*-wave superconductor. The Majorana zero mode (MZM) of such system may be applied for quantum computation through braiding, and certain experimental signature has been proposed in an ordinary *s*-wave superconducting wire with strong spin-orbital coupling through proximity effect^{5–13} or even in systems of ultracold atoms^{14–17}. However non-ambiguous evidence is still lacking probably due to the poor signal-to-noise ratio for a localized MZM. Recently, some extensions of Kitaev's 1D model by including inter-chain tunneling¹⁸, dimerization¹⁹, and long-ranged pairing^{20,21} have also been proposed.

However, in the traditional condensed matter systems, these interesting phases (nematic state, classical crystal, or quantum solid) cannot be achieved easily because the interaction strength has to be strong enough to compete with the Fermi energy. On the other hand, in the system of Rydberg atoms, the length scale and strength of the effective inter-atom interaction can be manipulated easily by external fields^{22–26}. In addition to the blockade effect for on-resonant excitations^{27–30}, one can also apply a far-detuned weak field (see Fig1 (a))

to generate an effective Rydberg-dressed interaction (RDI), which has a soft core and a finite interaction range (see in Fig1(b))^{31–33}. Theoretical calculations show that a repulsive RDI in a Bose gas may lead to a supersolid droplet phase^{31,32,34–36}, while an attractive RDI induces a 3D bright soliton³⁷. For a Rydberg Fermi gas, some topological phases are also predicted for an attractive³⁸ or repulsive interaction in a optical lattice near half-filling³⁹. Recently, Rydberg-dressed effective interaction has been observed for two individually trapped atoms⁴⁰ and in a 2D optical lattice by measuring the spin correlation⁴¹.

II. SYSTEM AND MODEL HAMILTONIAN

A. Effective Interaction:

In this paper, we consider a single-species Fermi gas, where each atom is weakly coupled to its *s*-wave Rydberg state by an off-resonant two photon transition via an intermediate state, see Fig.1(a). In the far detuning and weak coupling limit, we can apply the standard perturbative and adiabatic approximation³¹ to obtain the effective Rydberg-dressed interaction (RDI) between dressed state atoms: $V_{\text{RD}}(\mathbf{r}) = \frac{U_0}{1+(r/R_c)^6}$ ^{32,37,38,42}, where Ω and Δ are the effective Raman coupling and detuning respectively. $U_0 \equiv (\Omega/2\Delta)^4 C_6/R_c^6$, and $R_c \equiv (C_6/2|\Delta|)^{1/6}$ are the interaction strength and the averaged soft-core radius. C_6 is the averaged van der Waals coefficient, which can be shown to be positive for all orbital states when exciting ⁶Li or ⁴⁰K to a state with $n > 30$ ^{43,44}. The decay rate of the two photon process can be reduced by choosing larger detuning in the first transition, say $\Omega_1/\Delta_1 \ll 1$.

We note that the effective Rydberg-dressed interaction discussed above is more justified for the single-species Fermi gas³⁸ than for bosonic systems, because the Pauli exclusion principle can strongly reduce the possible atomic loss due to the orbital level crossing in the short-distance regime. As a result, we can calculate the scattering amplitude in 3D free space (valid in the weak interaction limit, $U_0/E_F^0 \ll k_F^0 R_c^{45}$) by the first Born approximation: $V(\mathbf{q}) \equiv \int d\mathbf{r} V_{\text{RD}}(\mathbf{r}) e^{-i\mathbf{q}\cdot\mathbf{r}} =$

FIG. 1. (a) Schematic plot for a two-photon excitation for an off-resonant coupling between the ground state ($|n_0S\rangle$) and a Rydberg state ($|n_2S\rangle$) via an intermediate state ($|n_1P\rangle$). $\Delta_{1,2}$ and $\Omega_{1,2}$ are the detuning and Rabi frequencies respectively. An effective single photon expression can be obtained with $\Delta = \Delta_1 + \Delta_2$ and $\Omega = \Omega_1\Omega_2/2\Delta_1$. (b) Effective Rydberg-dressed interaction in the far detuning limit ($\Delta \gg \Omega$) in the momentum space. The insert shows the corresponding real space profile with the blockade radius, R_c .

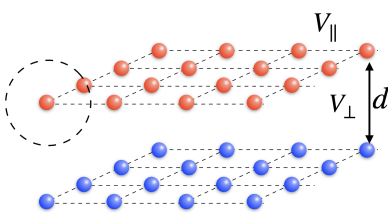


FIG. 2. The bilayer system with population imbalance of polar molecules.

$U_0 R_c^3 \tilde{V}(|\mathbf{q}|R_c)$, where

$$\tilde{V}(s) = \frac{2\pi^2}{3s} \left[1 + 2e^{s/2} \sin \left(\frac{\sqrt{3}s}{2} - \frac{\pi}{6} \right) \right] e^{-s}. \quad (1)$$

is a single-parameter function with $s \equiv |\mathbf{q}|R_c$. As shown in Fig.1(b), such scattering amplitude has a negative minimum at a finite wave vector, $|\mathbf{q}| = Q_c \sim 5.3/R_c$. This special property results from the blockade effects of the RDI in real space (see the inset), and does *not* exist in other kinds of long-ranged interaction, say Coulomb or dipolar interaction.

B. Hamiltonian

We consider identical fermionic polar molecules in a bilayer geometry with interlayer spacing d and tunneling amplitude t_z and the system setup is illustrated in Fig. 2. The full system Hamiltonian can be expressed as follows in the real-space coordinates:

$$H = \sum_{\mathbf{r}, \sigma=\uparrow, \downarrow} - \left[\mu c_{\mathbf{r}, \sigma}^\dagger c_{\mathbf{r}, \sigma} + t c_{\mathbf{r}, \sigma}^\dagger c_{\mathbf{r}+\hat{x}, \sigma} + t c_{\mathbf{r}, \sigma}^\dagger c_{\mathbf{r}+\hat{y}, \sigma} \right] + \sum_{\mathbf{r}} -t_z c_{\mathbf{r}, \uparrow}^\dagger c_{\mathbf{r}, \downarrow} + \frac{1}{2} \sum_{\mathbf{r}, \mathbf{r}'} \left[V_{\parallel}(\mathbf{r} - \mathbf{r}') \left(c_{\mathbf{r}, \uparrow}^\dagger c_{\mathbf{r}', \uparrow}^\dagger c_{\mathbf{r}', \uparrow} c_{\mathbf{r}, \uparrow} + c_{\mathbf{r}, \downarrow}^\dagger c_{\mathbf{r}', \downarrow}^\dagger c_{\mathbf{r}', \downarrow} c_{\mathbf{r}, \downarrow} \right) + V_{\perp}(\mathbf{r} - \mathbf{r}') \left(c_{\mathbf{r}, \uparrow}^\dagger c_{\mathbf{r}', \downarrow}^\dagger c_{\mathbf{r}', \downarrow} c_{\mathbf{r}, \uparrow} + c_{\mathbf{r}, \downarrow}^\dagger c_{\mathbf{r}', \uparrow}^\dagger c_{\mathbf{r}', \uparrow} c_{\mathbf{r}, \downarrow} \right) \right] \quad (2)$$

where $c_{\mathbf{r}}^\dagger(c_{\mathbf{r}, \sigma})$ is the creation (annihilation) operator of fermions for the layer index σ and the in-plane coordinate $\mathbf{r} = (i_x, i_y)$. μ is the chemical potential, the intra-layer hopping strength is t , and the interlayer hopping is t_z . V_{\perp} and V_{\parallel} are the interlayer and intra-layer interaction, respectively.

III. MEAN FIELD HAMILTONIAN AND SYMMETRY

A. Mean field Hamiltonian

By doing mean-field approximations and simplifying this model, the general mean field Hamiltonian is following:

$$H = \sum_{\mathbf{r}, \sigma=\uparrow, \downarrow} \left[-\mu c_{\mathbf{r}, \sigma}^\dagger c_{\mathbf{r}, \sigma} - t c_{\mathbf{r}, \sigma}^\dagger c_{\mathbf{r}+\hat{x}, \sigma} - t c_{\mathbf{r}, \sigma}^\dagger c_{\mathbf{r}+\hat{y}, \sigma} \right. \\ \left. + \Delta_x^\sigma c_{\mathbf{r}, \sigma}^\dagger c_{\mathbf{r}+\hat{x}, \sigma}^\dagger + \Delta_y^\sigma c_{\mathbf{r}, \sigma}^\dagger c_{\mathbf{r}+\hat{y}, \sigma}^\dagger + h.c. \right] \\ + \sum_{\mathbf{r}} \left[-t_z c_{\mathbf{r}, \uparrow}^\dagger c_{\mathbf{r}, \downarrow} + \Delta_z c_{\mathbf{r}, \uparrow}^\dagger c_{\mathbf{r}, \downarrow}^\dagger + h.c. \right] + \text{const.} \quad (3)$$

Δ_z is the gap function between the \uparrow and \downarrow layer on site \mathbf{r} and $\Delta_{x(y)}^\sigma$ with $\sigma = \uparrow, \downarrow$ are the in-plane gap function between nearest-neighboring sites by defining

$$\begin{aligned} \Delta_z &\equiv V_{\perp}(\mathbf{r} - \mathbf{r}') \langle c_{\mathbf{r}, \downarrow} c_{\mathbf{r}, \uparrow} \rangle, \\ \Delta_x^\sigma &\equiv V_{\parallel}(\hat{x}) \langle c_{\mathbf{r}+\hat{x}, \sigma} c_{\mathbf{r}, \sigma} \rangle, \\ \Delta_y^\sigma &\equiv V_{\parallel}(\hat{y}) \langle c_{\mathbf{r}+\hat{y}, \sigma} c_{\mathbf{r}, \sigma} \rangle. \end{aligned} \quad (4)$$

The controllable phase difference between Δ_x^σ and Δ_y^σ is the new feature compared with the $p_x \pm ip_y$ -wave pairing system. The constant is irrelevant for the following derivation of topological order and is omitted from now on. In order to simplify our model, here, we set

$$\Delta_x^\sigma = e^{i\phi_\sigma} |\Delta_p|, \quad \Delta_y^\sigma = ie^{i\alpha_\sigma} e^{i\phi_\sigma} |\Delta_p|. \quad (5)$$

We set \uparrow -layer and \downarrow -layer up to an arbitrary phase factor $e^{i\alpha_\uparrow}$, $e^{i\alpha_\downarrow}$, $e^{i\phi_\uparrow}$, and $e^{i\phi_\downarrow}$. In this paper, we would study how the relative phases of two orders effect the topological order. We also consider uniform pairing and hoping along z-direction: $\Delta_z = \Delta_s$. Δ_p and Δ_s are real.

This two spinless p-wave superconductor states with paring is similar to the p-wave superconductor with spin triplet pairing. It is instructive to first understand the bulk properties, which can be conveniently studied by imposing periodic boundary conditions on the system. We then make Fourier transform, $c_{\mathbf{r}, \sigma=\uparrow, \downarrow} = 1/N \sum_{\mathbf{k}} c_{\mathbf{k}, \sigma} e^{i\mathbf{r}\mathbf{k}}$ with $\mathbf{r} = (i_x, i_y)$, $\mathbf{k} = (k_x, k_y)$ and N is normalization factor. It takes the form $H = \sum_{\mathbf{k}} \Psi_{\mathbf{k}}^\dagger H(\mathbf{k}) \Psi_{\mathbf{k}}$, ignoring a constant, with

$$H(\mathbf{k}) = \begin{pmatrix} \varepsilon_{\mathbf{k}} & -t_z & (\tilde{\Delta}_{\mathbf{k}}^\uparrow)^\dagger & \Delta_s \\ -t_z & \varepsilon_{\mathbf{k}} & -\Delta_s & (\tilde{\Delta}_{\mathbf{k}}^\downarrow)^\dagger \\ \tilde{\Delta}_{\mathbf{k}}^\uparrow & -\Delta_s & -\varepsilon_{\mathbf{k}} & t_z \\ \Delta_s & \tilde{\Delta}_{\mathbf{k}}^\downarrow & t_z & -\varepsilon_{\mathbf{k}} \end{pmatrix} \quad (6)$$

and the Nambu spinor $\Psi_{\mathbf{k}} \equiv (c_{\mathbf{k}, \uparrow}, c_{\mathbf{k}, \downarrow}, c_{-\mathbf{k}, \uparrow}^\dagger, c_{-\mathbf{k}, \downarrow}^\dagger)^T$, Here, $c_{\mathbf{k}, \uparrow}(c_{\mathbf{k}, \downarrow})$ represents the electron annihilation operator with momentum \mathbf{k} and up (down)-layer and

$$\begin{aligned} \varepsilon_{\mathbf{k}} &= -\mu - 2t \cos k_x - 2t \cos k_y, \\ \tilde{\Delta}_{\mathbf{k}}^\sigma &= 2ie^{i\phi_\sigma} |\Delta_p| (\sin k_x + ie^{i\alpha_\sigma} \sin k_y). \end{aligned} \quad (7)$$

In the following, we would consider two cases: (1) symmetric case ($\alpha_\uparrow = 0, \alpha_\downarrow = 0$) and (2) anti-symmetric case ($\alpha_\uparrow = 0, \alpha_\downarrow = \pi$) with some particular phase factors (a) $\phi_\uparrow = \phi_\downarrow = 0$, (b) $\phi_\uparrow = \phi_\downarrow = \pi/2$, (b) $\phi_\uparrow = 0$ and $\phi_\downarrow = \pi$.

B. The system symmetry

The mean field Hamiltonian with momentum \mathbf{k} can be given by

$$H(\mathbf{k}) = \begin{pmatrix} H_0 & H_1^\dagger \\ H_1 & -H_0 \end{pmatrix}.$$

The diagonal term of H_1 and off diagonal term of H_1 are 2×2 matrices given by

$$H_0 = \begin{pmatrix} \varepsilon_{\mathbf{k}} & -t_z \\ -t_z & \varepsilon_{\mathbf{k}} \end{pmatrix}, \quad H_1 = \begin{pmatrix} \tilde{\Delta}_{\mathbf{k}}^\uparrow & -\Delta_s \\ \Delta_s & \tilde{\Delta}_{\mathbf{k}}^\downarrow \end{pmatrix}. \quad (8)$$

The normal part of the mean field Hamiltonian $H_0 = \varepsilon_{\mathbf{k}}\sigma_0 - t_z\sigma_x$ describes electrons on a square with kinetic term $\varepsilon_{\mathbf{k}} = -\mu - 2t \cos k_x - 2t \cos k_y$. σ_α ($\alpha = x, y, z$) are Pauli matrices, and $\sigma_0 = I$.

In particular, as $\phi_\uparrow = \phi_\downarrow$, the H_1 contains inter-layer (spin-singlet in spin language) and intra-layer (spin-triplet) pairing components

$$H_1 = (|\Delta_s|\sigma_0 + |\Delta_p|\mathbf{d}_\mathbf{k} \cdot \vec{\sigma})(i\sigma_y), \quad (9)$$

where $|\Delta_s|$ and $|\Delta_p|$ denote the interlayer and intra-layer pairing amplitudes, respectively and $\vec{\sigma}$ is the vector of Pauli matrices. The intra-layer pairing vector is $\mathbf{d}_\mathbf{k} = (0, 2\sin k_x + 2i\sin k_y, 0)$ as $\alpha_\uparrow = 0, \alpha_\downarrow = 0$. When $\alpha_\uparrow = 0, \alpha_\downarrow = \pi$, we have $\mathbf{d}_\mathbf{k} = (2\sin k_y, 2\sin k_x, 0)$.

We examine the symmetry class of the Hamiltonian, and consider the time-reversal symmetry (\mathcal{T}), particle-hole symmetry (\mathcal{P}), and chiral symmetry (\mathcal{C}) in the original BdG Hamiltonian, which are defined as,

$$\begin{aligned} \mathcal{T} H(\mathbf{k}) \mathcal{T}^\dagger &= H^*(-\mathbf{k}) \\ \mathcal{P} H(\mathbf{k}) \mathcal{P}^\dagger &= -H^T(-\mathbf{k}) \\ \mathcal{C} H(\mathbf{k}) \mathcal{C}^\dagger &= -H(\mathbf{k}) \end{aligned} \quad (10)$$

respectively. The representations of the time reversal (\mathcal{T}), the particle-hole reversal (\mathcal{P}), and the chiral (\mathcal{C}) operator are defined by

$$\begin{aligned} \mathcal{T} &= \sigma_0 \otimes i\sigma_y, \quad \mathcal{T}^2 = -1 \\ \mathcal{P} &= \sigma_x \otimes \sigma_0, \quad \mathcal{P}^2 = 1 \\ \mathcal{C} &= \mathcal{P}\mathcal{T}^\dagger = (\sigma_x \otimes \sigma_0)(\sigma_0 \otimes -i\sigma_y). \end{aligned} \quad (11)$$

In particular, the chiral superconductor with $p_x + ip_y$ pairing breaks time reversal symmetry. However, if $\alpha_\uparrow = 0$ and $\alpha_\downarrow = \pi$ in bilayer system, this is to generalize the chiral pairing state to the helical pairing superconducting state, where fermions with up layer (up-spins) are paired in the $p_x + ip_y$ state, and fermions with down layer (down-spins) are paired in the $p_x - ip_y$ state. Such system may have time reversal symmetry, $\mathcal{T} H(\mathbf{k}) \mathcal{T}^{-1} = H(-\mathbf{k})$. The BdG Hamiltonian that conserves the time reversal symmetry is described by

$$\begin{pmatrix} i\sigma_y & 0 \\ 0 & i\sigma_y \end{pmatrix} H(\mathbf{k}) \begin{pmatrix} -i\sigma_y & 0 \\ 0 & -i\sigma_y \end{pmatrix} = H^*(-\mathbf{k}). \quad (12)$$

The time reversal symmetry conserves only at $t_z = 0$, $\phi_\uparrow = -\phi_\downarrow$, and $\alpha_\uparrow = \pi + \alpha_\downarrow$, and the model is a time-reversal

invariant topological superconductor in the DIII class (up layer is labeled as \uparrow and down layer is labeled as \downarrow).

To simplify our discussion, we consider some particular cases and the summary of the mean field Hamiltonian with gapless region and symmetries is shown in Table I.

$\alpha_\uparrow = 0, \alpha_\downarrow = 0$	$\phi_\uparrow = \phi_\downarrow = 0$	$\phi_\uparrow = \phi_\downarrow = \pi/2$	$\phi_\uparrow = 0, \phi_\downarrow = \pi$
$\Delta_s \neq 0, t_z = 0$	\mathcal{P} (D)	\mathcal{P} (D)	\mathcal{P} (D)
$t_z \neq 0$	\mathcal{P} (D)	\mathcal{P} (D)	\mathcal{P} (D)*
$\alpha_\uparrow = 0, \alpha_\downarrow = \pi$	$\phi_\uparrow = \phi_\downarrow = 0$	$\phi_\uparrow = \phi_\downarrow = \pi/2$	$\phi_\uparrow = 0, \phi_\downarrow = \pi$
$\Delta_s \neq 0, t_z = 0$	$\mathcal{T} \mathcal{P} \mathcal{C}$ (DIII)*	\mathcal{P} (D)	\mathcal{P} (D)
$t_z \neq 0$	\mathcal{P} (D)*	\mathcal{P} (D)*	\mathcal{P} (D)*

TABLE I. The symmetry and symmetry class of Hamiltonian. There is a gapless region from energy spectra filling by yellow.

IV. TOPOLOGICAL PROPERTIES

A. Topological index

To expose the topological invariant that distinguishes these phases, consider a 2D superconductor described by a Hamiltonian of the form $H(\mathbf{k}) = \mathbf{h}(\mathbf{k}) \cdot \vec{\sigma}$ with $\mathbf{h}(\mathbf{k})$ a smooth function that is non-zero for all momenta so that the bulk is fully gapped. One can then define a unit vector $\hat{\mathbf{h}}(\mathbf{k})$ that maps 2D momentum space onto a unit sphere.

Assuming that $\hat{\mathbf{h}}(\mathbf{k})$ tends to a unique vector as $|\mathbf{k}| \rightarrow \infty$ (independent of the direction of \mathbf{k}), the number of times this map covers the entire unit sphere defines an integer topological invariant given formally by the Chern number

$$C = \int \frac{d^2k}{4\pi} [\hat{\mathbf{h}}(\mathbf{k}) \cdot (\partial_{k_x} \hat{\mathbf{h}}(\mathbf{k}) \times \partial_{k_y} \hat{\mathbf{h}}(\mathbf{k}))] \quad (13)$$

The integrand above determines the solid angle (which can be positive or negative) that $\hat{\mathbf{h}}(\mathbf{k})$ sweeps on the unit sphere over an infinitesimal patch of momentum space centered on \mathbf{k} . Performing the integral over all \mathbf{k} yields an integer that remains invariant under smooth deformations of $\hat{\mathbf{h}}(\mathbf{k})$. The Chern number can change only when the gap closes, making $\hat{\mathbf{h}}(\mathbf{k})$ ill-defined at some momentum.

B. Entanglement spectrum

Besides of the Chern number, a topological phase can be also characterized by the quantum entanglement between the subsystem and the environment^{46–50}. Given a ground state wave function $|\Psi\rangle$, one can calculate the reduced density matrix, ρ_A , for a subsystem A by tracing over the environment. The eigenvalues λ_α of the reduced density matrix is so-called “entanglement spectrum”⁴⁸, which carries nonlocal information and has been applied for calculating Berry phase and

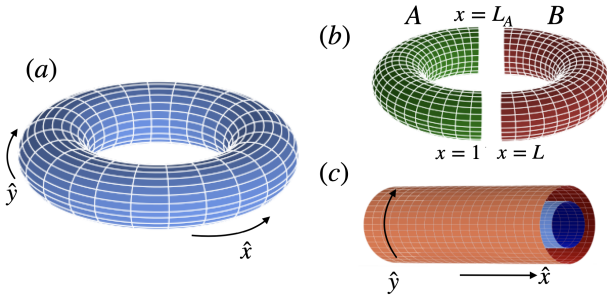


FIG. 3. (a) The bilayer system with periodic boundary condition from a torus. (b) The torus is cut along a loop in the y direction into two cylinder. (c) When cut into two “half cylinders,” we find a localized edge state near the boundary.

zero-energy edge states⁵¹. For example, the degeneracy of the entanglement spectrum has recently implemented to characterize the topological orders for some 2D quantum Hall states and for some 1D SPT phases⁴⁸.

For 1D Kitaev model, λ_α is given by the eigenvalues of the block Green’s function matrix, i.e., $G_{i,j} \equiv \langle c_i c_j^\dagger \rangle$ with the layer indices i and j inside the subsystem A . In Ref.^{51–53}, it has been shown that the zero energy mode of the 1D Kitaev model corresponds to the degeneracy of $\lambda_\alpha = 1/2$ in the entanglement spectrum, i.e. the pair of zero modes at the two ends of Kitaev’s chain contribute the maximal entanglement between the subsystem A and environment. Besides of entanglement spectrum, a topological phase transition can be also identified by the entanglement entropy of the subsystem (given by $S_A = -Tr\rho_A \log \rho_A$) after tracing out the environment.

It has been shown that the entanglement spectrum λ_α of the subsystem A can be obtained by diagonalizing the entire Green’s function matrix $G_{\mathbf{r}_1, \sigma_1, \mathbf{r}_2, \sigma_2}$ ^{51–53}, where (\mathbf{r}_1, σ_1) and (\mathbf{r}_2, σ_2) are restricted in the subsystem A .

When a 2D translational invariant system is bipartitioned by a 1D chain, we can perform the 1D Fourier transformation along the interface. We can divide our system into two parts along x - or y -direction, and keep another direction with translation symmetry. The Hamiltonian is block-diagonal in terms of the wave number k_y (or k_x), $H = \sum_{k_y} H_{k_y}$ (or $H = \sum_{k_x} H_{k_x}$), where $H(k_y)$ (or $H(k_x)$) is a 1D Hamiltonian for each k_y (or k_x) subspace. For example, we choose interface along x -direction and obtain $H = \sum_{k_y} H_{k_y}$. The entire Green’s function matrix of wave number k_y is given by

$$G(k_y)_{x_1, \sigma_1, x_2, \sigma_2} = \frac{1}{L} \sum_{k_x, k_y \in BZ} e^{ik_x(x_1-x_2)} G(k_x, k_y)_{\sigma_1, \sigma_2} \quad (14)$$

where L is the number site of x -direction and k_x, k_x takes values in the Brillouin zone. $G(k_x, k_y)_{\sigma_1, \sigma_2}$ is a 4×4 matrix determined by the eigenvectors of mean-field Hamiltonian Eq. 6.

In our case, we numerically diagonalize the block’s Green’s function for subsystem A with a finite size, e.g., $L_A = 20$ and $L = 40$ as shown in Fig. 3. The numerical results converges and is independent of the choices of subsystem in the thermal

dynamic limit, $L \gg L_A \gg 1$. In Figs. 4, we show the entanglement spectra λ_α and entanglement entropy S_A obtained by calculating the Green’s function from the effective Hamiltonian. The topological regime for $\lambda_\alpha = 1/2$ appears through a topological phase transition at which, the entanglement entropy diverges. In Figs. 4, we show the regime of topological non-trivial phase ($\lambda_\alpha = 1/2$), which is exactly the same regime from energy spectra.

C. Topological edge mode

In this section, we investigate edge state for our bilayer system numerically. From the bulk-edge correspondence, a non-trivial bulk topological phase will imply the existence of gapless edge states. For 2D systems with edges, we first Fourier transform along a direction parallel to the edge to get a family of 1D Hamiltonians parametrized by the wave number along the edge. It is instructive to understand the edge properties, which can be conveniently studied by imposing open boundary conditions on the system. We then make Fourier transform along y -direction, $c_{x,y,\sigma} = 1/\sqrt{N_y} \sum_{k_y} e^{ik_y} c_{k_y,x,\sigma}$ and N_y is normalization factor on Hamiltonian Eq. 3. An effective Bogoliubov-de Gennes (BdG) Hamiltonian can be easily derived to be $H_{\text{BdG}} = \sum_{k_y} H_{k_y}$, where

$$\begin{aligned} H_{k_y} = & \sum_{x,\sigma=\uparrow,\downarrow} \left[(-\mu - 2t \cos k_y) c_{x,k_y,\sigma}^\dagger c_{x,k_y,\sigma} \right. \\ & - tc_{x,k_y,\sigma}^\dagger c_{x+1,k_y,\sigma} + e^{i\phi_\sigma} \Delta_p c_{x,k_y,\sigma}^\dagger c_{x+1,-k_y,\sigma} \\ & \left. + ie^{i\alpha_\sigma} e^{i\phi_\sigma} \Delta_p e^{ik_y} c_{x,k_y,\sigma}^\dagger c_{x,-k_y,\sigma} + h.c. \right] \\ & + \sum_x \left[-t_z c_{x,k_y,\uparrow}^\dagger c_{x,k_y,\downarrow} + \Delta_s c_{x,k_y,\uparrow}^\dagger c_{x,-k_y,\downarrow} + h.c. \right] \end{aligned} \quad (15)$$

One can see that, we can that define

$$H_{k_y}^{\text{four-leg}} = H_{k_y} + H_{-k_y} \quad (16)$$

is a four-leg chain in momentum k_y space. Otherwise, we also can make Fourier transform along x -direction and get $H_{\text{BdG}} = \sum_{k_x} H_{k_x}$ with

$$\begin{aligned} H_{k_x} = & \sum_{y,\sigma=\uparrow,\downarrow} \left[(-\mu - 2t \cos k_x) c_{k_x,y,\sigma}^\dagger c_{k_x,y,\sigma} \right. \\ & - tc_{k_x,y,\sigma}^\dagger c_{k_x,y+1,\sigma} + e^{i\phi_\sigma} \Delta_p e^{ik_x} c_{k_x,y,\sigma}^\dagger c_{-k_x,y,\sigma} \\ & \left. + ie^{i\alpha_\sigma} e^{i\phi_\sigma} \Delta_p c_{x,k_y,\sigma}^\dagger c_{x,-k_y,\sigma} + h.c. \right] \\ & + \sum_x \left[-t_z c_{x,k_y,\uparrow}^\dagger c_{x,k_y,\downarrow} + \Delta_s c_{x,k_y,\uparrow}^\dagger c_{x,-k_y,\downarrow} + h.c. \right] \end{aligned} \quad (17)$$

Suppose that the system has two boundary edges, i.e., at $x = 1$ and $x = L$ and impose the periodic boundary condition in the y direction. By solving the energy spectrum as a function of the momentum k_y numerically, we could study edge states. We may consider the subject under the following head: (a) gap closing condition; (b) topological number and entanglement

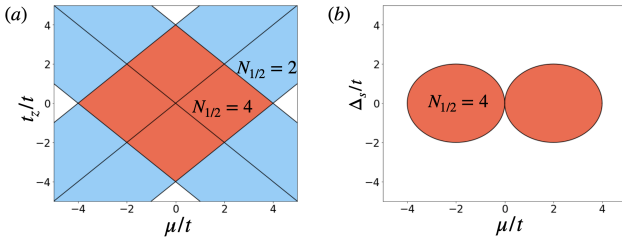


FIG. 4. Phase diagram of Hamiltonian Eq. (6) for $\alpha_\uparrow = \alpha_\downarrow = 0$ and $\phi_\uparrow = \phi_\downarrow = 0$ fixed (a) $|\Delta_s|/t = 0$ and (b) $t_z/t = 0$. $N_{1/2}$ is the number of the degenerate entanglement spectrum at $\lambda_\alpha = 1/2$ in the subsystem A , also indicating the number of Majorana Zero Modes pairs at the edge (with open boundaries at $x = 1$ and $x = 20$).

entropy; (c) edge state. In the following, it will be useful, to begin with, to make a distinction between two kinds of (1) $\alpha_\uparrow = \alpha_\downarrow = 0$; (2) $\alpha_\uparrow = 0$ $\alpha_\downarrow = \pi$.

V. PHASE DIAGRAM OF SYMMETRIC CASE ($\alpha_\uparrow = \alpha_\downarrow = 0$)

In general, a phase transition between phases occur only when the energy gap of the bulk spectrum closes. Thus, to identify parameter regions for which different (topological phases) are realized, we would first examine the bulk spectrum of the system. To obtain the bulk spectrum, we would adopt periodic boundary condition (PBC) to form bulk Hamiltonian and study the phase boundary. On the other hand, from the bulk-edge correspondence, a nontrivial bulk topological number implies the existence of gapless edge states. To investigate edge states, we would open edges along one direction to form a family of 1D Hamiltonians parametrized by wave number k . For example, by solving numerically the energy spectrum as a function of the momentum k_y in the y direction, we could study edge states near the interface.

First of all, it is easy to calculate the the energy eigenvalues of the bulk Hamiltonian for such a symmetric case with $\alpha_\uparrow = \alpha_\downarrow = 0$. To simplify our system, we shall confine our attention to two special point: $|\Delta_s|/t = 0$ and $t_z/t = 0$ for the present with special phase factor conditions (See Table. II). In the following, we would show the details for energy spectra and entanglement spectra.

	$\Delta_s/t = 0$	$t_z/t = 0$
$\phi_\uparrow = \phi_\downarrow = 0$	$\sin k_x = \sin k_y = 0$	$\sin k_x = \pm \frac{ \Delta_s }{2 \Delta_p }; \sin k_y = 0$
$\phi_\uparrow = \phi_\downarrow = \pi/2$	$\sin k_x = \sin k_y = 0$	$\sin k_x = 0; \sin k_y = \pm \frac{ \Delta_s }{2 \Delta_p }$
$\phi_\uparrow = 0, \phi_\downarrow = \pi$		$\sin k_x = 0; \sin k_y = \pm \frac{ \Delta_s }{2 \Delta_p }$

TABLE II. Gap closing condition

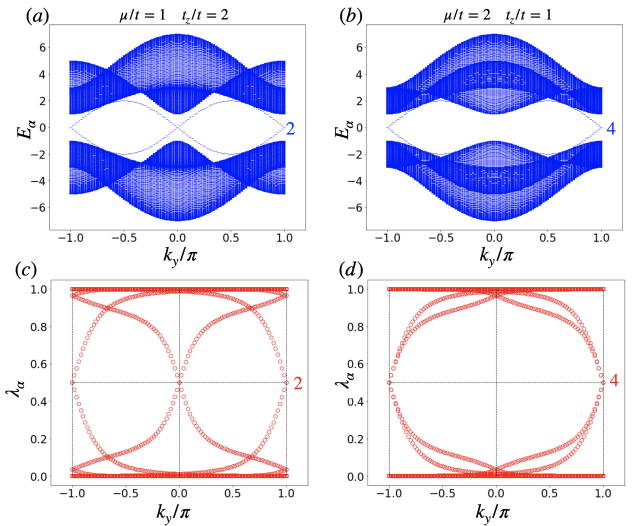


FIG. 5. The energy spectra as a function of k_y (the momentum in y direction), $k_y \in [0, 2\pi]$ with finite size $L = 100$ with boundaries at $x = 1$ and $x = 100$. The chemical potential and interlayer hopping are (a) $\mu/t = 1, t_z/t = 2$ and (b) $\mu/t = 2, t_z/t = 2$. The corresponding spectra of the reduced density with cut at $x = 1$ and $x = 50$ are shown in (c) $\mu/t = 1, t_z/t = 2$ and (d) $\mu/t = 2, t_z/t = 2$.

A. For $\phi_\uparrow = \phi_\downarrow = 0$

A simple evaluation shows that the eigenvalues of matrix (Eq. 6) with zero interlayer coupling are simply $\pm E_{\mathbf{k}}$, where

$$E_{\mathbf{k}} = \left[\varepsilon_{\mathbf{k}}^2 + t_z^2 + 4|\Delta_p|^2 (\sin^2 k_x + \sin^2 k_y) + |\Delta_s|^2 \right. \\ \left. \pm 2\sqrt{\varepsilon_{\mathbf{k}}^2 t_z^2 + t_z^2 |\Delta_s|^2 + 4|\Delta_p|^2 |\Delta_s|^2 \sin^2 k_x} \right]^{1/2}.$$

In our model, the gap of the system closes only when the following condition is satisfied:

$$\varepsilon_{\mathbf{k}}^2 + t_z^2 + 4|\Delta_p|^2 (\sin^2 k_x + \sin^2 k_y) + |\Delta_s|^2 = \\ 2\sqrt{\varepsilon_{\mathbf{k}}^2 t_z^2 + t_z^2 |\Delta_s|^2 + 4|\Delta_p|^2 |\Delta_s|^2 \sin^2 k_x} \quad (18)$$

We examine the gap closing condition using Eq. (18) for zero interlayer coupling ($|\Delta_s|/t = 0$) and zero interlayer hopping ($t_z/t = 0$).

Zero interlayer coupling $|\Delta_s|/t = 0$. From a straightforward calculation, it is found that the gap closes at $\mathbf{k} = (k_x, k_y) = (0, 0), (0, \pi), (\pi, 0), (\pi, \pi)$. Substituting these (k_x, k_y) values into Eq. (18), we get the gap closing conditions,

$$t_z = \pm \mu, \quad t_z = \pm (\mu + 2t), \quad t_z = \pm (\mu - 2t) \quad (19)$$

When one of above equations is satisfied, the energy gap closes. Then, there are at most sixteen regions of parameter space as shown in Fig. 4(a). We will explore the properties of states with these different regions.

To study edge states, we impose the periodic boundary condition in the y direction. Fourier transforming along the y direction and obtain a family of 1D Hamiltonians parametrized

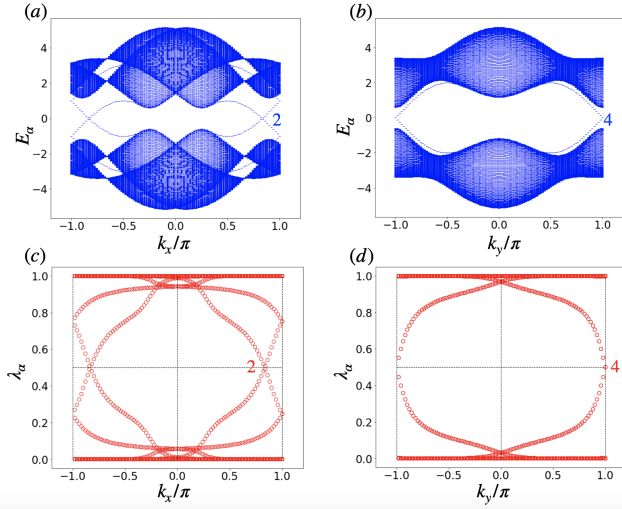


FIG. 6. (a) The energy spectra as a function of k_x (the momentum in x direction) $k_x \in [0, 2\pi]$ with finite size $L = 100$ with boundaries at $y = 1$ and $y = L$ for $\mu/t = 1$, $|\Delta_s|/t = 1$. Panel (b) is the same as (a) but as a function of k_y . The corresponding spectra of the reduced density with open edges (c) at $y = 1$ and $y = L/2$ and (d) at $x = 1$ and $x = L/2$.

by k_y . Suppose that the system has two open boundary edges at $x = 1$ and $x = L$. By solving numerically the energy spectrum as a function of the momentum k_y in the y direction, we study edge states. Figs 5(a) and (b) show the energy spectra with open boundaries along x axis and translational invariance along the y direction. It shows zero energy modes appear for $k_y = 0$ or $k_y = \pi$. On the other hand, these edge states contribute to the entanglement entropy. The corresponding spectra of the reduced density with open ends is shown in Figs. 5(c) and (d). These results are consistent with the bulk-edge correspondence again.

Zero interlayer hopping $t_z/t = 0$. Again, the gap of the system closes only when the following condition is satisfied:

$$\varepsilon_{\mathbf{k}}^2 = 4|\Delta_p|^2 \sin^2 k_y = \left(|\Delta_s| \pm 2|\Delta_p| \sin k_x \right)^2 = 0. \quad (20)$$

From a straightforward calculation, it is found that the gap closes at $\sin k_x = \pm \frac{|\Delta_s|}{2|\Delta_p|}$ and $\sin k_y = 0$. Substituting these (k_x, k_y) values into Eq. (20), we get the gap closing conditions,

$$\left(\frac{\mu}{t} \pm 2 \right)^2 |\Delta_p|^2 + |\Delta_s|^2 = 4|\Delta_p|^2$$

In this case, all of the gap closing conditions from two circle with radius 2 shown in Fig. 4(b).

In Fig. 4(a)(b), we show the entanglement spectra λ_α and entanglement entropy S_A obtained by calculating the Green's function from the effective Hamiltonian. We find that the ground state becomes topologically non-trivial ($\lambda_\alpha = 1/2$) at exactly the same regime as Eq. (20) and Eq. (18). The entanglement entropy becomes divergent when cross the boundary. These edge state contribute to degenerate entanglement spectrum at $\lambda_\alpha = 1/2$. These numerical results agree with the

analytic calculation of the winding number, confirming the topological properties in our current system.

In particular, if $|\Delta_s|/t = 0$ and $t_z/t = 0$, the Hamiltonian reduces to a bilayer chiral p-wave superconductor without interlayer interaction. There are four phases separated by three quantum critical points at $\mu/t = 0, \pm 4$, which are labeled by the Chern number (Ch) as Ch= 0 ($|\mu/t| > 4$), Ch= -1 ($-4 < \mu/t < 0$), and Ch= 1 ($0 < \mu/t < 4$).

B. For $\phi_\uparrow = \phi_\downarrow = \pi/2$

A simple evaluation shows that the eigenvalues of matrix (Eq. 6) with zero interlayer coupling are simply $\pm E_{\mathbf{k}}$, where

$$E_{\mathbf{k}} = \left[\varepsilon_{\mathbf{k}}^2 + t_z^2 + 4|\Delta_p|^2 (\sin^2 k_x + \sin^2 k_y) + |\Delta_s|^2 \pm 2\sqrt{\varepsilon_{\mathbf{k}}^2 t_z^2 + t_z^2 |\Delta_s|^2 + 4|\Delta_p|^2 |\Delta_s|^2 \sin^2 k_y} \right]^{1/2}$$

The analysis is the same as the case of Sec. V.A.

C. For $\phi_\uparrow = 0, \phi_\downarrow = \pi$

A simple evaluation shows that the eigenvalues of matrix (Eq. 6) with zero interlayer coupling are simply given

$$E_{\mathbf{k}} = t_z \pm \left[\varepsilon_{\mathbf{k}}^2 + 4|\Delta_p|^2 \sin^2 k_x + (2|\Delta_p| \sin k_y - |\Delta_s|)^2 \right]^{1/2}$$

$$E_{\mathbf{k}} = -t_z \pm \left[\varepsilon_{\mathbf{k}}^2 + 4|\Delta_p|^2 \sin^2 k_x + (2|\Delta_p| \sin k_y + |\Delta_s|)^2 \right]^{1/2}$$

Zero interlayer coupling $|\Delta_s|/t = 0$. The gap of the system closes only when the following condition is satisfied:

$$t_z^2 = [\varepsilon_{\mathbf{k}}^2 + 4|\Delta_p|^2 (\sin^2 k_x + \sin^2 k_y)]$$

In this case, all of the gap closing conditions depend on not only Hamiltonian parameters but also the momentum k_x and k_y . **some special case!! I am checking it**

Zero interlayer hopping $t_z/t = 0$. Again, the gap of the system closes only when the following condition is satisfied:

$$\varepsilon_{\mathbf{k}}^2 = 4|\Delta_p|^2 \sin^2 k_x = \left(|\Delta_s| \pm 2|\Delta_p| \sin k_y \right)^2 = 0.$$

Again, we can find that the gap close at $\sin k_x = 0$ and $\sin k_y = \pm \frac{|\Delta_s|}{2|\Delta_p|}$ which is similar to $\phi_\uparrow = \phi_\downarrow = 0$ case by rotated 90 degree.

VI. PHASE DIAGRAM OF ANTI-SYMMETRIC CASE ($\alpha_\uparrow = 0, \alpha_\downarrow = \pi$)

We then consider anti-symmetric case ($\alpha_\downarrow = \pi$). Again, to simplify our system, we first confine our attention to two special points: (1) $|\Delta_s|/t = 0$ and (2) $t_z/t = 0$ for the present.

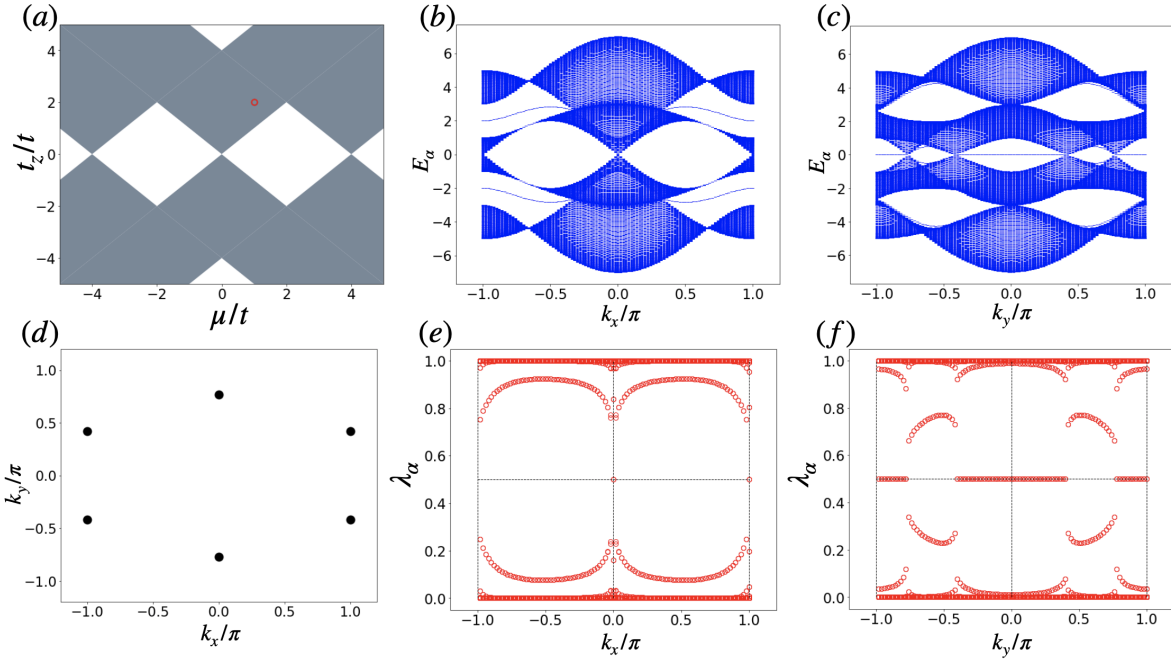


FIG. 7. (a) The gapless point (grey region) as computed via the energy eigenvalue of bulk Hamiltonian in $t = |\Delta_p|$ for $|\Delta_s|/t = 0$ $\phi_\uparrow = \phi_\downarrow = 0$ and $\alpha_\uparrow = 0$ $\alpha_\downarrow = \pi$. Panel (b) shows the energy spectra with open edges at $y = 1$ and $y = L$ as a function of k_x , $k_x \in [0, 2\pi)$ for $\mu/t = 1$, $|\Delta_s|/t = 0$, and $t_z/t = 2$. Panel (c) is the same as (b) but as a function of k_y with open edges at $x = 1$ and $x = L$. (d) The energy gap of the bulk spectrum closes at k_x^* and k_y^* for $\mu/t = 1$, $|\Delta_s|/t = 0$, and $t_z = 2/t$. The corresponding spectra of the reduced density with open edges (e) at $y = 1$ and $y = L/2$ and (f) at $x = 1$ and $x = L/2$.

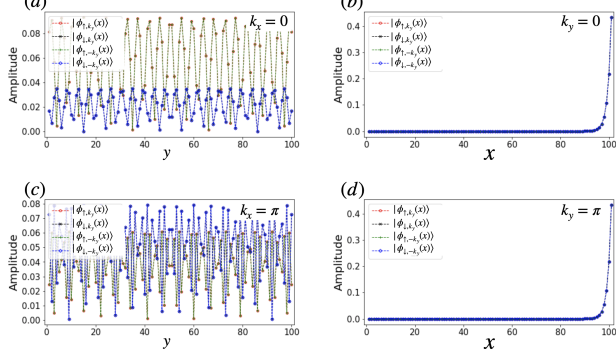


FIG. 8. We take $\mu/t = 1$, $|\Delta_s|/t = 0$, and $t_z/t = 2$ with open boundaries at $x = 1$ and $x = 100$ ((a)) $k_x = 0$, (c) $k_x = \pi$), with open boundaries at $y = 1$ and $y = 100$ (b)(d). (b) and (d) illustrate the wave function of Majorana modes localized around $y = 100$ for (b) $k_y = 0$ and (d) $k_y = \pi$. The amplitude of the layer-resolved wave function is shown.

A. For $\phi_\uparrow = \phi_\downarrow = 0$

A simple evaluation shows that the eigenvalues of matrix with zero interlayer coupling are simply $\pm E_{\mathbf{k}}$.

Zero interlayer coupling $|\Delta_s|/t = 0$. To simplify the Hamiltonian, we first consider the zero interlayer coupling.

Diagonalizing the BdG Hamiltonian, we find

$$E_{\mathbf{k}} = \pm \left[\left(\sqrt{\varepsilon_{\mathbf{k}}^2 + 4|\Delta_p|^2 \sin^2 k_y} \pm t_z \right)^2 + 4|\Delta_p|^2 \sin^2 k_x \right]^{1/2}.$$

In this model, the gap of the system closes only when the following condition is satisfied:

$$4|\Delta_p|^2 \sin^2 k_x = \left(\sqrt{\varepsilon_{\mathbf{k}}^2 + 4|\Delta_p|^2 \sin^2 k_y} \pm t_z \right)^2 = 0$$

Therefore, the gap closes at $k_x = 0$ or $k_x = \pi$ (see Fig. 7 (d)). From a straightforward calculation, it is found that this condition is equivalent to

$$(-\mu/t \mp 2)^2 + 4 - 2(-\mu/t \mp 2) \cos k_y = (t_z/t)^2 \quad (21)$$

where “-” term corresponds to $k_x = 0$, “+” term corresponds to $k_x = \pi$, and k_y is related to the lattice size. This is, the gap of the system closes at \mathbf{k} which is determined by Hamiltonian parameters (see Fig. 7 (a)).

The energy spectrum of the family of Hamiltonian $H(k_y)$ parametrized by the wave number in the y -direction, k_y , is given in Fig. 7 (c) with periodic boundary condition. We can see where the energy gap close (see Fig. 7 (d)). The energy spectrum as a function of k_y with open edge at $x = 1$ and $x = L$ show in Fig. 7(c) and show this model may hold the Majorana zero modes at each end. We can see that two pairs of Majorana zero modes appear at some k'_y 's.

As $t_z/t = 0$, the zero modes appear at $\sin k_x = 0$ and four-fold degeneracy entanglement spectrum (see Fig. 9(a)). This is a gaped topological order phase. In Fig. 7(a), we see some region with gapless point at $k'_y s$ from Eqs. (21). In particular, we can see the edge state with zero energy modes appear (see Fig. 8) during gapless points with open edge at $x = 1$ and $x = L$. Otherwise, there is no zero energy edge modes with open edge at $y = 1$ and $y = L$. This could be a gapless topological order phase.

Zero interlayer hopping $t_z/t = 0$. It is easy to check that for such a anti-symmetric case, the energy eigenvalues of bulk Hamiltonian are

$$E_{\mathbf{k}} = \pm \left[\varepsilon_{\mathbf{k}}^2 + \left(|\Delta_s| \pm 2|\Delta_p| \sqrt{\sin^2 k_x + \sin^2 k_y} \right)^2 \right]^{1/2}$$

as expected. Again, the gap of the system closes only when the following condition is satisfied:

$$\varepsilon_{\mathbf{k}}^2 = \left(|\Delta_s| \pm 2|\Delta_p| \sqrt{\sin^2 k_x + \sin^2 k_y} \right)^2 = 0$$

It is found that this condition is equivalent to

$$\begin{aligned} \cos^2 k_x + \cos^2 k_y &= 2 - |\Delta_s|^2 / 4t^2 \\ \cos k_x + \cos k_y &= -\mu / 2t \end{aligned} \quad (22)$$

It is obvious to see that if $\mathbf{k} = (k_x, k_y)$ is a generic solution, $(\pm k_x, \pm k_y)$ and $(\pm k_y, \pm k_x)$ are also solutions, i.e. there are eight-fold degeneracy, belong to C_{4v} group (see Fig. 10(d)).

The energy spectrum of the family of Hamiltonians $H(k_x)$ and k_y parametrized by the wave number is given in Fig. 10(b)(c). Again, with open edges, this model may hold the Majorana zero modes at each end. In Fig. 10(b)(c), we show the energy spectrum at gapless phases with $\mu/t = 1$ and $|\Delta_s|/t = 2$. The gap closes at $k'_y s$ from Eqs. (22).

In particular, if $|\Delta_s|/t = 0$ and $t_z/t = 0$, the Hamiltonian reduces to a bilayer chiral p-wave superconductor without inter-layer interaction. It is known that there are four phases separated by three quantum critical points at $\mu/t = 0, \pm 4$, which are labeled by the Chern number. On the other hand, we also calculate the entanglement spectrum and show the number of degenerate $N_{1/2}$ in Fig. 4(b), which is same as the symmetric case. This is, there is no Majorana zero modes at gapless region. In order to understand which phase is these gapless phases, we study the values of k_x and k_y at bulk gap closure. In Fig. 10(b)(c), the system admits gapless bulk excitations only when the momentum k_x and k_y is fine tuned. This transition point is from topological order phase to gapless phase.

B. For $\phi_{\uparrow} = \phi_{\downarrow} = \pi/2$

A simple evaluation shows that the eigenvalues of matrix with zero interlayer coupling are simply $\pm E_{\mathbf{k}}$, where

$$\begin{aligned} E_{\mathbf{k}} = \pm \left[\varepsilon_{\mathbf{k}}^2 + t_z^2 + 4|\Delta_p|^2 (\sin^2 k_x + \sin^2 k_y) + |\Delta_s|^2 \right. \\ \left. \pm 2|t_z| \sqrt{\varepsilon_{\mathbf{k}}^2 + |\Delta_s|^2 + 4|\Delta_p|^2 \sin^2 k_y} \right]^{1/2} \end{aligned}$$

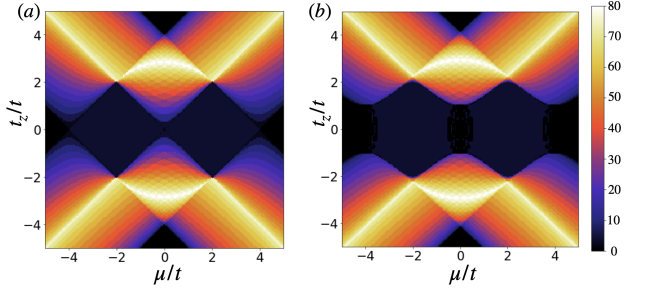


FIG. 9. Phase diagram of Eq. (6) as a function of μ/t and t_z/t for (a) $|\Delta_s|/t = 0$ and (b) $|\Delta_s|/t = 1$ with $\alpha_{\uparrow} = 0$ $\alpha_{\downarrow} = \pi$ and $\phi_{\uparrow} = \phi_{\downarrow} = 0$. $N_{1/2}$ is the number of the degenerate entanglement spectrum at $\lambda_{\alpha} = 1/2$ with lattice size 40×40 and cut system along x-direction.

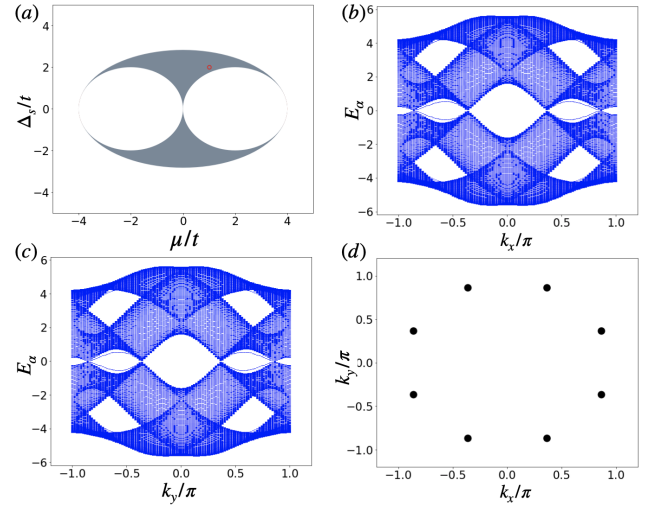


FIG. 10. (a) The phase boundary (black line) and gapless point (grey region) as computed via the energy eigenvalue for $t_z/t = 0$, $\phi_{\uparrow} = \phi_{\downarrow} = 0$ and $\alpha_{\uparrow} = 0$ $\alpha_{\downarrow} = \pi$ with under periodic boundary condition. Panel (b) shows the energy spectrum as a function of k_x , $k_x \in [0, 2\pi]$ for the bilayer system under periodic boundary condition with finite size $L = 100$ with $\mu/t = 1$, $|\Delta_s|/t = 2$, and $t_z/t = 0$. The lower eigenstates is represented by the red line under the open (periodic) boundary condition for the y (x) direction, respectively. Panel (c) is the same as (b) but as a function of k_y and the red line under the open boundary condition for the x direction. (d) The bulk gap closes at particular momentum k_x^* and k_y^* (belong to C_{4v} group) for $\mu/t = 1$, $|\Delta_s|/t = 1$, and $t_z/t = 0$.

Zero interlayer coupling $|\Delta_s|/t = 0$. The gap of the system closes only when the following condition is satisfied:

$$4|\Delta_p|^2 \sin^2 k_x = \left(\sqrt{\varepsilon_{\mathbf{k}}^2 + 4|\Delta_p|^2 \sin^2 k_y} \pm t_z \right)^2 = 0$$

In this case, all of the gap closing conditions depend on not only Hamiltonian parameters but also the momentum k_x and k_y .

Zero interlayer hopping $t_z/t = 0$. Again, the gap of the

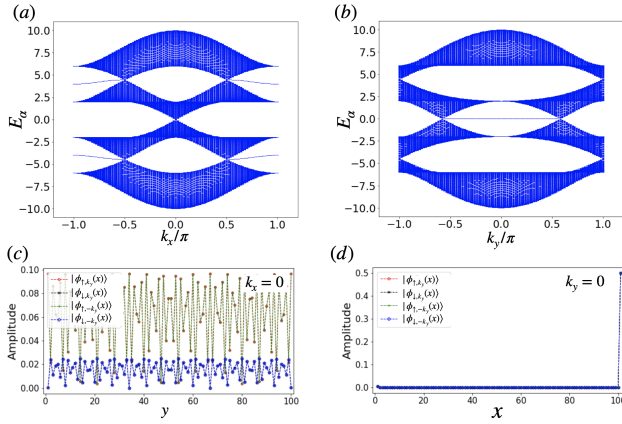


FIG. 11. (a) The energy spectra as a function of k_x (the momentum in x direction) $k_x \in [0, 2\pi]$ with finite size $L = 100$ with boundaries at $y = 1$ and $y = L$ for $\mu/t = 1$, $|\Delta_s|/t = 1$. Panel (b) is the same as (a) but as a function of k_y . Panel (c) shows the amplitude of the layer-resolved wave function with open boundaries at $x = 1$ and $x = 100$. Panel (d) is the same as (c) but as a function of y .

system closes only when the following condition is satisfied:

$$\varepsilon_{\mathbf{k}}^2 = 4|\Delta_p|^2(\sin^2 k_x + \sin^2 k_y)^2 = |\Delta_s|^2 = 0.$$

Again, we can find that the gap close only at $|\Delta_s| = 0$ and $\mu = 0, \pm 4$ at $\mathbf{k} = (0, 0), (0, \pi), (\pi, 0), (\pi, \pi)$.

C. For $\phi_\uparrow = 0$ $\phi_\downarrow = \pi$

A simple evaluation shows that the eigenvalues of matrix with zero interlayer coupling are simply $\pm E_{\mathbf{k}}$, where

$$E_{\mathbf{k}} = \pm \left[\varepsilon_{\mathbf{k}}^2 + t_z^2 + 4|\Delta_p|^2 (\sin^2 k_x + \sin^2 k_y) + |\Delta_s|^2 \right. \\ \left. \pm 2|t_z| \sqrt{\varepsilon_{\mathbf{k}}^2 + |\Delta_s|^2 + 4|\Delta_p|^2 \sin^2 k_x} \right]^{1/2}$$

Zero interlayer coupling $|\Delta_s|/t = 0$. The gap of the system closes only when the following condition is satisfied:

$$4|\Delta_p|^2 \sin^2 k_y = \left(\sqrt{\varepsilon_{\mathbf{k}}^2 + 4|\Delta_p|^2 \sin^2 k_x} \pm t_z \right)^2 = 0$$

In this case, all of the gap closing conditions depend on not only Hamiltonian parameters but also the momentum k_x and k_y .

Zero interlayer hopping $t_z/t = 0$. Again, the gap of the system closes only when the following condition is satisfied:

$$\varepsilon_{\mathbf{k}}^2 = 4|\Delta_p|^2(\sin^2 k_x + \sin^2 k_y)^2 = |\Delta_s|^2 = 0.$$

Again, we can find that the gap close only at $|\Delta_s| = 0$ and $\mu = 0, \pm 4$ at $\mathbf{k} = (0, 0), (0, \pi), (\pi, 0), (\pi, \pi)$.

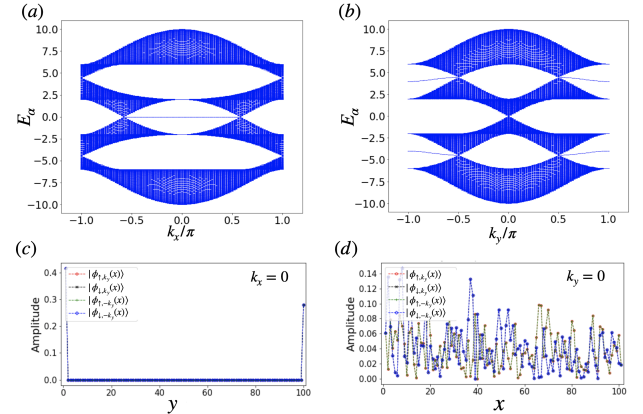


FIG. 12. (a) The energy spectra as a function of k_x (the momentum in x direction) $k_x \in [0, 2\pi]$ with finite size $L = 100$ with boundaries at $y = 1$ and $y = L$ for $\mu/t = 1$, $|\Delta_s|/t = 1$. Panel (b) is the same as (a) but as a function of k_y . Panel (c) shows the amplitude of the layer-resolved wave function with open boundaries at $x = 1$ and $x = 100$. Panel (d) is the same as (c) but as a function of y .

VII. CONCLUSION

ACKNOWLEDGMENTS

This work was supported by the MOST of Taiwan under Grants No. 108-2112-M-029 -006 -MY3.

Appendix A: The Hamiltonian in Majorana fermion basis

We then note that the definition of Majorana fermions (MFs) in real space is different from that in momentum space. Therefore, by doing Fourier Transformation, the Majorana operators in momentum space can be given

$$\begin{aligned} c_{x,k_y,\sigma} &= \frac{1}{2} \left[\gamma_{x,k_y,\sigma}^{(1)} + i \gamma_{x,k_y,\sigma}^{(2)} \right], \\ c_{x,k_y,\sigma}^\dagger &= \frac{1}{2} \left[\gamma_{x,-k_y,\sigma}^{(1)} - i \gamma_{x,-k_y,\sigma}^{(2)} \right], \\ c_{x,-k_y,\sigma} &= \frac{1}{2} \left[\gamma_{x,-k_y,\sigma}^{(1)} + i \gamma_{x,-k_y,\sigma}^{(2)} \right], \\ c_{x,-k_y,\sigma}^\dagger &= \frac{1}{2} \left[\gamma_{x,k_y,\sigma}^{(1)} - i \gamma_{x,k_y,\sigma}^{(2)} \right] \end{aligned} \quad (\text{A1})$$

For example, in two dimensions, the simplest system that realizes a topological phase supporting Majorana fermions is a spinless 2D electron gas exhibiting $p_x + ip_y$ superconductivity and defined by

$$\begin{aligned} H = & -\mu \sum_{x,y=1}^L c_{x,y}^\dagger c_{x,y} - \sum_{x,y=1}^L t [c_{x,y}^\dagger c_{x+1,y} + c_{x,y}^\dagger c_{x,y+1} + h.c.] \\ & - \sum_{x,y=1}^L [\Delta c_{x,y}^\dagger c_{x+1,y}^\dagger + i\Delta c_{x,y}^\dagger c_{x,y+1}^\dagger + h.c.] \end{aligned}$$

There are four phases separated by three quantum critical points at $\mu = 0, \pm 4$, which are labeled by the Chern number (Ch) as paired states in the fractional quantum Hall effect: $Ch = 0$ ($|\mu| > 4$), $Ch = -1$ ($-4 < \mu < 0$), and $Ch = +1$ ($0 < \mu < 4$).

The Hamiltonian is block-diagonal in terms of the wave number along the interface k_y , $H = \sum_{k_y} H_{k_y}$, where H_{k_y} is a 1D Hamiltonian for each k_y subspace. We then consider $\Delta = t = 1$ and the Hamiltonian with Majorana fermion basis can be given by

$$\begin{aligned} H_k = & -\frac{1}{2} \sum_{x=1}^L \left[\frac{i}{2} (\mu + 2t_y \cos k) \left(\gamma_{x,-k}^{(1)} \gamma_{x,k}^{(2)} - \gamma_{x,-k}^{(2)} \gamma_{x,k}^{(1)} \right) \right. \\ & + \frac{i}{2} t_x \left(\gamma_{x,-k}^{(1)} \gamma_{x+1,k}^{(2)} - \gamma_{x,-k}^{(2)} \gamma_{x+1,k}^{(1)} + \gamma_{x,k}^{(1)} \gamma_{x+1,-k}^{(2)} - \gamma_{x,k}^{(2)} \gamma_{x+1,-k}^{(1)} \right) \\ & - \frac{i}{2} |\Delta_p| \left(\gamma_{x,-k}^{(1)} \gamma_{x+1,k}^{(2)} + \gamma_{x,-k}^{(2)} \gamma_{x+1,k}^{(1)} + \gamma_{x,k}^{(1)} \gamma_{x+1,-k}^{(2)} + \gamma_{x,k}^{(2)} \gamma_{x+1,-k}^{(1)} \right) \\ & \left. + |\Delta_p| \sin k \left(\gamma_{x,-k}^{(1)} \gamma_{x,k}^{(1)} + \gamma_{x,k}^{(2)} \gamma_{x,-k}^{(2)} \right) \right] \end{aligned} \quad (\text{A2})$$

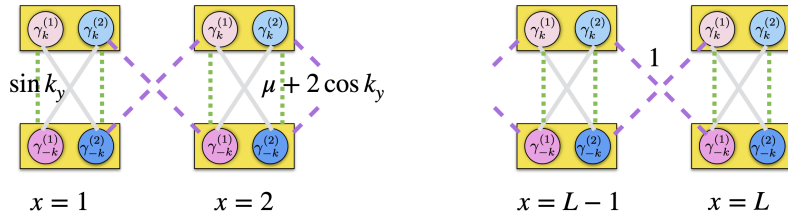


FIG. 13. The Hamiltonian with Majorana fermion basis

The Majorana fermions occur at boundary if only if $\sin k_y = 0$. For 1D dimerized model, the gapless phase occurs at bond with equal weight. So, we have $|\mu \pm 2| = 2$ and the gapless point occur at $\mu = 0, \pm 4$.

¹ E. Majorana, Il Nuovo Cimento (1924-1942) **14**, 171 (2008).

² C.-K. Chiu, J. C. Y. Teo, A. P. Schnyder, and S. Ryu, Rev. Mod.

- Phys. **88**, 035005 (2016).
- ³ M. Cheng, M. Zaletel, M. Barkeshli, A. Vishwanath, and P. Bonderson, Phys. Rev. X **6**, 041068 (2016).
 - ⁴ A. Y. Kitaev, Physics-Uspekhi **44**, 131 (2001).
 - ⁵ L. Fu and C. L. Kane, Phys. Rev. Lett. **100**, 096407 (2008).
 - ⁶ J. D. Sau, R. M. Lutchyn, S. Tewari, and S. Das Sarma, Phys. Rev. Lett. **104**, 040502 (2010).
 - ⁷ J. Alicea, Phys. Rev. B **81**, 125318 (2010).
 - ⁸ M. Sato, Y. Takahashi, and S. Fujimoto, Phys. Rev. B **82**, 134521 (2010).
 - ⁹ R. M. Lutchyn, J. D. Sau, and S. Das Sarma, Phys. Rev. Lett. **105**, 077001 (2010).
 - ¹⁰ V. Mourik, K. Zuo, S. M. Frolov, S. R. Plissard, E. P. A. M. Bakkers, and L. P. Kouwenhoven, Science **336**, 1003 (2012).
 - ¹¹ A. Das, Y. Ronen, Y. Most, Y. Oreg, M. Heiblum, and H. Shtrikman, Nature Physics **8**, 887 (2012).
 - ¹² L. X. F. J. K. Rokhinson, Leonid P., Nature Physics **8**, 795 (2012).
 - ¹³ M. T. Deng, C. L. Yu, G. Y. Huang, M. Larsson, P. Caroff, and H. Q. Xu, Nano Letters **12**, 6414 (2012).
 - ¹⁴ S. Tewari, S. Das Sarma, C. Nayak, C. Zhang, and P. Zoller, Phys. Rev. Lett. **98**, 010506 (2007).
 - ¹⁵ Z. Shermadini, A. Krzton-Maziopa, M. Bendele, R. Khasanov, H. Luetkens, K. Conder, E. Pomjakushina, S. Weyeneth, V. Pomjakushin, O. Bossen, and A. Amato, Phys. Rev. Lett. **106**, 117602 (2011).
 - ¹⁶ X.-J. Liu, K. T. Law, and T. K. Ng, Phys. Rev. Lett. **112**, 086401 (2014).
 - ¹⁷ M. Sato, Y. Takahashi, and S. Fujimoto, Phys. Rev. Lett. **103**, 020401 (2009).
 - ¹⁸ R. Wakatsuki, M. Ezawa, and N. Nagaosa, Phys. Rev. B **89**, 174514 (2014).
 - ¹⁹ R. Wakatsuki, M. Ezawa, Y. Tanaka, and N. Nagaosa, Phys. Rev. B **90**, 014505 (2014).
 - ²⁰ A. Alecce and L. Dell'Anna, Phys. Rev. B **95**, 195160 (2017).
 - ²¹ D. Vodola, L. Lepori, E. Ercolessi, A. V. Gorshkov, and G. Pupillo, Phys. Rev. Lett. **113**, 156402 (2014).
 - ²² Y. O. Dudin and A. Kuzmich, Science **336**, 887 (2012).
 - ²³ U. Raitzsch, V. Bendkowsky, R. Heidemann, B. Butscher, R. Löw, and T. Pfau, Phys. Rev. Lett. **100**, 013002 (2008).
 - ²⁴ J. D. Pritchard, D. Maxwell, A. Gauguet, K. J. Weatherill, M. P. A. Jones, and C. S. Adams, Phys. Rev. Lett. **105**, 193603 (2010).
 - ²⁵ J. Nipper, J. B. Balewski, A. T. Krupp, B. Butscher, R. Löw, and T. Pfau, Phys. Rev. Lett. **108**, 113001 (2012).
 - ²⁶ P. Schauß, M. Cheneau, M. Endres, T. Fukuhara, S. Hild, A. Omran, T. Pohl, C. Gross, S. Kuhr, and I. Bloch, Nature **491**, 87 (2012).
 - ²⁷ D. Jaksch, J. I. Cirac, P. Zoller, S. L. Rolston, R. Côté, and M. D. Lukin, Phys. Rev. Lett. **85**, 2208 (2000).
 - ²⁸ M. D. Lukin, M. Fleischhauer, R. Cote, L. M. Duan, D. Jaksch, J. I. Cirac, and P. Zoller, Phys. Rev. Lett. **87**, 037901 (2001).
 - ²⁹ E. Urban, T. A. Johnson, T. Henage, L. Isenhower, D. D. Yavuz, T. G. Walker, and M. Saffman, Nature Physics **5**, 110 (2009).
 - ³⁰ A. Gaëtan, Y. Miroshnychenko, T. Wilk, A. Chotia, M. Viteau, D. Comparat, P. Pillet, A. Browaeys, and P. Grangier, Nature Physics **5**, 115 (2009).
 - ³¹ N. Henkel, R. Nath, and T. Pohl, Phys. Rev. Lett. **104**, 195302 (2010).
 - ³² N. Henkel, F. Cinti, P. Jain, G. Pupillo, and T. Pohl, Phys. Rev. Lett. **108**, 265301 (2012).
 - ³³ J. B. Balewski, A. T. Krupp, A. Gaj, S. Hofferberth, R. Löw, and T. Pfau, New Journal of Physics **16**, 063012 (2014).
 - ³⁴ H. P. Büchler, E. Demler, M. Lukin, A. Micheli, N. Prokof'ev, G. Pupillo, and P. Zoller, Phys. Rev. Lett. **98**, 060404 (2007).
 - ³⁵ F. Cinti, P. Jain, M. Boninsegni, A. Micheli, P. Zoller, and G. Pupillo, Phys. Rev. Lett. **105**, 135301 (2010).
 - ³⁶ G. Pupillo, A. Micheli, M. Boninsegni, I. Lesanovsky, and P. Zoller, Phys. Rev. Lett. **104**, 223002 (2010).
 - ³⁷ F. Maucher, N. Henkel, M. Saffman, W. Królikowski, S. Skupin, and T. Pohl, Phys. Rev. Lett. **106**, 170401 (2011).
 - ³⁸ B. Xiong, H. H. Jen, and D.-W. Wang, Phys. Rev. A **90**, 013631 (2014).
 - ³⁹ X. Li and S. D. Sarma, Nature Communications **6**, 7137 (2015).
 - ⁴⁰ Y.-Y. Jau, A. M. Hankin, T. Keating, I. H. Deutsch, and G. W. Biedermann, Nature Physics **12**, 71 (2016).
 - ⁴¹ J. Zeiher, R. van Bijnen, P. S. S. Hild, T. P. Jae-yoon Choi, I. Bloch, and C. Gross, arXiv: 1602.06313 (2013).
 - ⁴² J. Honer, H. Weimer, T. Pfau, and H. P. Büchler, Phys. Rev. Lett. **105**, 160404 (2010).
 - ⁴³ T. G. Walker and M. Saffman, Phys. Rev. A **77**, 032723 (2008).
 - ⁴⁴ K. Singer, M. Reetz-Lamour, T. Amthor, S. Fölling, M. Tschernecker, and M. Weidemüller, **38**, S321 (2005).
 - ⁴⁵ L. D. Landau, *Quantum Mechanics*.
 - ⁴⁶ A. Kitaev and J. Preskill, Phys. Rev. Lett. **96**, 110404 (2006).
 - ⁴⁷ M. Levin and X.-G. Wen, Phys. Rev. Lett. **96**, 110405 (2006).
 - ⁴⁸ H. Li and F. D. M. Haldane, Phys. Rev. Lett. **101**, 010504 (2008).
 - ⁴⁹ F. Pollmann, A. M. Turner, E. Berg, and M. Oshikawa, Phys. Rev. B **81**, 064439 (2010).
 - ⁵⁰ A. M. Turner, F. Pollmann, and E. Berg, Phys. Rev. B **83**, 075102 (2011).
 - ⁵¹ S. Ryu and Y. Hatsugai, Phys. Rev. B **73**, 245115 (2006).
 - ⁵² M.-C. Chung, Y.-H. Jhu, P. Chen, and S. Yip, EPL (Europhysics Letters) **95**, 27003 (2011).
 - ⁵³ M.-C. Chung, Y.-H. Jhu, P. Chen, and C.-Y. Mou, Journal of Physics: Condensed Matter **25**, 285601 (2013).